



Plasmonic Properties of Gold Nanostructures on Gold Film

Médéric Lequeux^{1,2} · David Mele¹ · Priyamvada Venugopalan^{3,4} · Raymond Gillibert¹ · Souhir Boujday² · Wolfgang Knoll³ · Jakub Dostalek³ · Marc Lamy de la Chapelle⁵ 

Received: 22 January 2020 / Accepted: 5 May 2020 / Published online: 26 May 2020
© Springer Science+Business Media, LLC, part of Springer Nature 2020

Abstract

This paper reports on a systematic study of the plasmonic properties of periodic arrays of gold cylindrical nanoparticles in contact with a gold thin film. Depending on the gold film thickness, it observes several plasmon bands. Using a simple analytical model, it is able to assign all these modes and determine that they are due to the coupling of the grating diffraction orders with the propagating surface plasmons travelling along the film. With finite difference time domain (FDTD) simulations, it demonstrates that large field enhancement occurs at the surface of the nanocylinders due to the resonant excitation of these modes. By tilting the sample, it also observes the evolution of the spectral position of these modes and their tuning through nearly the whole visible range is possible. Such plasmonic substrates combining both advantages of the propagative and localised surface plasmons could have large applications in enhanced spectroscopies.

Keywords Plasmonics · Gold thin film · Grating · Gold nanostructures

Introduction

Plasmonic substrates composed of metallic nanostructures in intimate contact with metallic film of nanometric thickness exhibit some specific plasmonics properties owing to both localised surface plasmon (LSP) as well as propagative surface plasmons (PSP) [1].

Several studies have been provided in the literature concerning the coupling between metallic nanostructures and metallic film. They essentially focus on the use of a

spacing layer to separate the nanostructures from the film. When the nanostructures are randomly distributed on the spacing layer surface, the coupling with the metallic film has only an influence on the position of the LSP resonance of the nanoparticles with a strong redshift when the nanostructure/film gap decreases [2, 3]. Such redshift, which can be higher than 100 nm for gap lower than 1 nm, is related with the gap distance and could be used to probe the nanostructures/film distance with high precision [3]. Some waveguide modes in the spacing layer have also been observed [4]. It has also been demonstrated that such configuration induces the formation of a highly enhanced field in the spacing layer depending on the gap distance [5, 6].

To obtain a coupling between LSP and PSP, it is necessary that the nanostructures form a grating on the metallic film or spacing layer surface. Indeed, if the nanostructures are prepared in a regular manner in form of periodic arrays, there are introduced new wave vectors directly related to the grating parameters and to the appearance of diffraction orders of the grating. These wave vectors can be used to excite the plasmon modes supported by the film and the grating structure depending notably on its orientation with respect to the direction of excitation optical wave.

In the case of the use of a spacing layer, some simulations have shown that, in addition to the LSP resonance, it is possible to observe the (1;1) and (1;0) PSP modes of the metallic film inducing an improvement of the surface plasmon

Electronic supplementary material The online version of this article (<https://doi.org/10.1007/s11468-020-01185-9>) contains supplementary material, which is available to authorized users.

✉ Marc Lamy de la Chapelle
marc.lamydelachapelle@univ-lemans.fr

¹ Sorbonne Paris Cité, Laboratoire CSPBAT, CNRS, (UMR 7244), Université Paris 13, 74 rue Marcel Cachin, 93017 Bobigny, France

² Laboratoire LRS, CNRS-UPMC UMR 7197, Université Pierre et Marie Curie, 4 place Jussieu, 75005 Paris, France

³ Biosensor Technologies, AIT-Austrian Institute of Technology GmbH, Konrad-Lorenz-Strasse 24., 3430 Tulln, Austria

⁴ CEST Kompetenzzentrum für elektrochemische Oberflächentechnologie GmbH, TFZ, Wiener Neustadt, Viktor-Kaplan-Strasse 2., 2700 Wiener Neustadt, Austria

⁵ IMMM-UMR 6283 CNRS, Le Mans Université, Avenue Olivier Messiaen, 72085 Le Mans Cedex 9, France

resonance (SPR) sensitivity [7, 8]. Strong coupling has also been observed with the formation of hybrid modes and anti-crossing behaviour on the LSP and PSP resonances [9, 10].

When the nanostructure grating is in direct contact with the gold film, the substrate acts as a single plasmonic system exhibiting specific properties through the excitation of Bragg modes corresponding to the resonant coupling of the plasmon modes travelling along the plane of the array periodicity [1, 11–14].

Detailed experimental studies of such plasmonic substrates have already been done by Hohenau et al. [15, 16] on gold nanosquare grating at the surface of gold film. They were then able to highlight the observation of the (1,0) and (1,1) modes propagating at the air/gold interface. Two photon luminescence (TPL) and FDTD simulations were also used to map and calculate the field enhancement induced at the surface of such substrates. It shows a strong localisation of the near field on the edges of the nanostructures. Moreover, such configuration exhibits some advantages and confers to the substrate some specific plasmonic properties as demonstrated previously [17–26]. Firstly, it has been demonstrated that such substrate improves the spatial resolution in surface plasmon resonance imaging (SPRI) or the SPR sensitivity [17–19]. Furthermore, these modes were investigated for surface plasmon-enhanced spectroscopy applications [20]. They provide a higher Raman intensity in surface enhanced Raman scattering (SERS) compared to the one recorded for identical metallic nanostructures on dielectric substrates (glass or ITO, indium tin oxide) [21–24]. A gain of one order of magnitude has been reported [21]. The surface-enhanced Raman scattering (SERS) signal exhibits also a directivity depending on the grating period and corresponding to the coupling of both incident and Raman scattering wave vectors with the grating [25]. Finally, the field enhancement distribution and localisation at the vicinity of the substrate surface are completely different from the one observed for similar nanostructures on dielectric surface [26]. In the case of the thin film, the field distribution is more homogeneous on the whole surface of the film and of the nanostructures whereas for the nanostructures on dielectric, the field is more localised at the top and the edge of the metallic nanostructures [26].

In view of all these specificities, it is then of utmost importance to gain a deep understanding of the properties of these substrates in order to be able to tailor them for real applications such as enhanced optical spectroscopies [27–32] or sensing [33–35] as the plasmon modes are directly involved in the performance characteristics of such methods.

However, in the previous studies, the influence of the metallic film thickness was never studied. Only the thickness of the spacing layer, the size and shape of the nanostructures or the grating period were modified [2, 4, 5, 8, 15, 16]. Moreover, the thickness used by Hohenau et al. [16] is too large to allow the excitation of the plasmon modes at the

interface between the gold and the substrate. As shown in this paper, for thickness lower than 50 nm, we have been able to probe and study such plasmon modes. As well, no modification of the \mathbf{k} vector was performed through angular study or specific illumination configuration that gives access to different plasmon energy and can be used to probe the plasmon modes along the dispersion curve.

In this paper, we present a detailed study of such Bragg modes depending on (i) the thickness of the gold thin film in order to determine the influence of the dispersion curve of plasmon modes travelling along the film and (ii) the incidence angle in order to study the shift of the Bragg modes with the wave vector value (Fig. 1). Based on an analytical model reproducing the grating-plasmon coupling, we are then able to identify precisely each Bragg mode. We also determine the field distribution at the vicinity of the surface and inside the film using finite difference time domain (FDTD) simulations and its evolution with the film thickness.

Results and Discussion

Our plasmonic substrate is composed of square arrays (periodicity, Λ , of 400 nm) of gold nanocylinders on a flat gold thin film (Fig. 1). The nanocylinder diameters (D) were varied from 80 to 250 nm whereas the nanocylinder height, h , is fixed at 50 nm. Four different film thicknesses, d_m , were used: 20, 30, 40, and 50 nm. The measured extinction spectra of the samples are shown in Fig. 2 for several nanocylinder diameters and for different gold film thicknesses.

One can notice that for one specific thickness, the spectral position of the plasmon bands (peaks observed on the extinction spectrum) is constant for varying diameters. The only observable change is the band intensity depending on the diameter D , which could be attributed to the increase in the quantity of gold matter as the diameter increases. On contrary, the number and the spectral position of the bands are strongly affected by the gold film thickness d_m as shown in the Fig. 3. The band at the longest wavelength (between 650 and 700 nm) is slightly blue-shifted when the thickness d_m increases. Similar behaviour is also observed for the band located at wavelength of around 600 nm but with a larger slope (Fig. 3b). This latter one seems to merge with the band that appears around 530 nm for a thickness of 30 nm.

These modes can be easily assigned using an analytical model describing diffraction coupling to the PSP travelling along a gold thin film. The nanocylinder grating is assumed to be a perturbation and the spectrum of PSP modes is solved for a thin gold film (refractive index n_m) with a thickness d_m sandwiched between air (refractive index n_a) and glass (refractive index n_g). The propagation constant of transverse magnetically (TM) polarised PSP modes β was determined by numerically solving the dispersion relation:

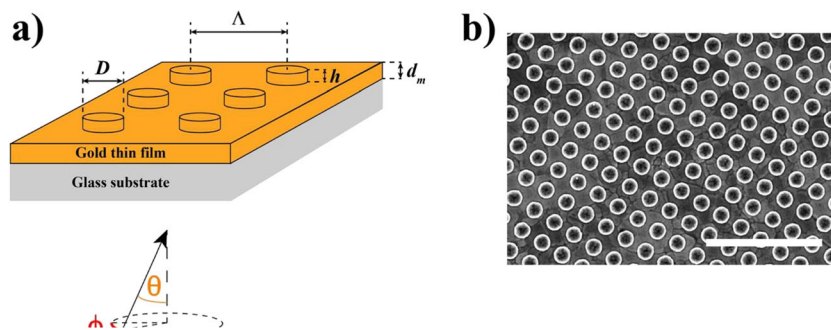


Fig. 1 **a** Scheme of the plasmonic substrate including gold nanocylinders deposited on a gold thin film (D : nanocylinder diameter, h : nanocylinder height, Λ : grating period, d_m : film thickness) and of the illumination

configuration (θ : incidence polar angle and ϕ : azimuthal angle; $\theta = 0^\circ$ and $\phi = 0^\circ$ in normal incidence). **b** SEM image of nanocylinders with a diameter of 250 nm on a gold film (scale bar = 2 μm)

$$\tan(k_0 \kappa d_m) - \frac{\frac{\kappa}{n_m^2} \left(\frac{\gamma_g}{n_g^2} + \frac{\gamma_a}{n_a^2} \right)}{\frac{\kappa^2}{n_m^4} - \frac{\gamma_g \gamma_a}{n_g^2 n_a^2}} = 0 \tag{1}$$

that was derived from Maxwell equations with respective boundary conditions. $k_0 = 2\pi/\lambda$ is the wavenumber of light in vacuum for a wavelength λ , and transverse propagation constants were set to $\kappa = (\beta^2 - k_0^2 n_m^2)^{1/2}$, $\gamma_a = (\beta^2 - k_0^2 n_a^2)^{1/2}$, $\gamma_g = (\beta^2 - k_0^2 n_g^2)^{1/2}$. In general, gold thin film supports one guided TM_0 mode that in the limit of large thickness d_m corresponds to the PSP mode at the glass substrate/gold interface. In addition, a TM_1 PSP mode travels at the opposite interface (air/gold interface). It is leaky to the glass medium, and in the limit of large thickness d_m , it corresponds to the PSP mode at the air/gold interface. The simulated dispersion relation of TM_0 PSP mode is presented in Fig. 4 as a function of its effective refractive index $\text{Re}\{\beta\}/k_0$ on the wavelength λ . It

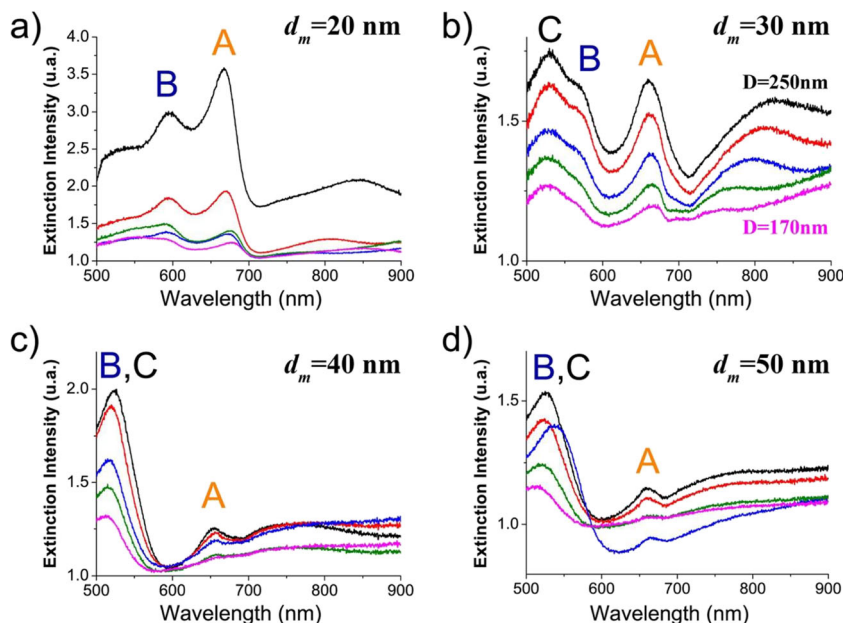
shows that it reaches its maximum at a wavelength of about 520 nm; it sharply drops when decreasing the wavelength to 500 nm and slowly decreases with increasing wavelength to near infrared part of spectrum. The real part of the TM_0 propagation constant $\text{Re}\{\beta\}$ increases when decreasing the thickness of the film d_m and it is much higher than that for the second PSP mode TM_1 .

Diffraction coupling of a light beam propagating in the far field to PSP modes occurs when the following phase matching condition is fulfilled:

$$k_0 \sqrt{\left(n_a \sin[\theta] \sin[\phi] + m \frac{\lambda}{\Lambda} \right)^2 + \left(n_a \sin[\theta] \cos[\phi] + n \frac{\lambda}{\Lambda} \right)^2} = \text{Re}\{\beta\} \tag{2}$$

where θ is the polar angle, ϕ is the azimuthal angle of incidence and integers (m, n) are the diffraction orders. For the normal angle of incidence $\theta = 0^\circ$ and period $\Lambda = 400$ nm, the

Fig. 2 Extinction spectra for different gold film thicknesses, d_m : 20 nm (a), 30 nm (b), 40 nm (c), and 50 nm (d), and different nanocylinder diameters, D (black spectra: 250 nm, red spectra: 230 nm, blue spectra: 210 nm, green spectra: 190 nm and pink spectra: 170 nm). The A, B and C plasmon bands correspond to the resonance identified on the Fig. 4



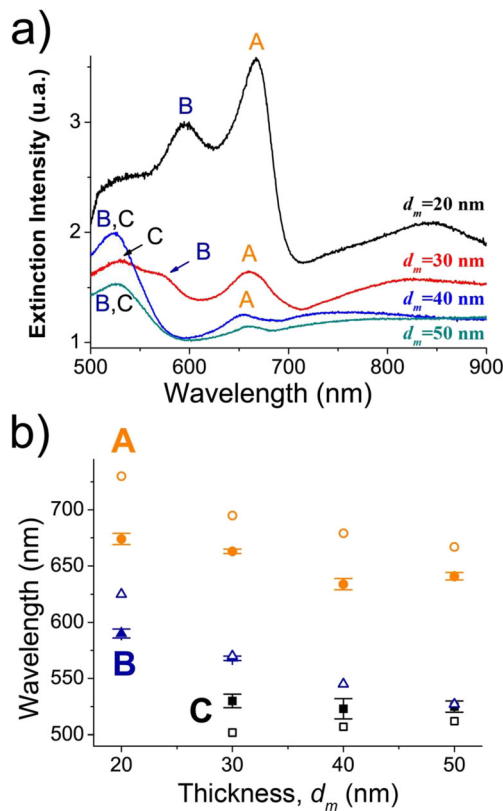


Fig. 3 **a** Extinction spectra for nanocylinders with a diameter of 250 nm and for different gold film thicknesses (black spectrum: 20 nm, red spectrum: 30 nm, blue spectrum: 40 nm, green spectrum: 50 nm). **b** Evolution of the experimental (plain symbols) and theoretical (void symbols) position of the plasmon bands with the gold film thickness, d_m , and their assignment based on the analytical model (equation 1). The A, B and C plasmon bands correspond to the resonance identified on the Fig. 4

first diffraction orders $(0, \pm 1)$ and $(\pm 1, 0)$ are presented as a dashed line in Fig. 4. In addition, the second diffraction orders $(\pm 1, \pm 1)$ are showed as dotted line. These orders intersect the dispersion relation of TM_0 modes in three spectral regions, which correspond to three distinct resonances marked as A, B and C. The resonance A originates from the first diffraction order coupling. Resonances B and C are due to the second order coupling, which is predicted to cut the dispersion relation twice due to the peak occurring in PSP dispersion relation. For the selected period Λ , no resonance due to the excitation of PSP mode TM_1 occurs. The evolutions of these three modes with the thickness reproduce perfectly the ones observed experimentally: (i) a blue-shift for the two modes at longer wavelengths with a higher shift for the lowest one and (ii) a merging of the two modes at the lowest wavelengths for the higher thicknesses (Fig. 3b).

We can then assign the longest wavelength mode (resonance A) to the $(0, \pm 1)$ and $(\pm 1, 0)$ modes, whereas the two shorter wavelength ones (resonances B and C) are assigned to the $(\pm 1, \pm 1)$ modes (Fig. 3).

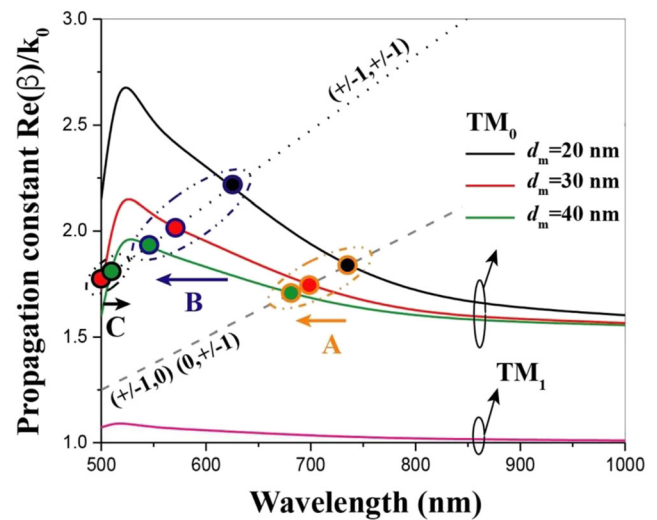


Fig. 4 Dispersion curves calculated with the analytical model (equation 1) for different gold film thicknesses, d_m , for the TM_0 mode (black curve: 20 nm, red curve: 30 nm and green curve: 40 nm) and TM_1 mode (pink curve simulated for $d_m \rightarrow \infty$). The dashed line corresponds to the $(\pm 1, 0)$ or $(0, \pm 1)$ diffraction order whereas the dotted line corresponds to the $(\pm 1, \pm 1)$ diffraction order (equation 2). The colour dots indicate the phase matching between the diffraction orders and the dispersion curves for the resonances A, B and C

In order to gain a better understanding of the characteristics of these modes, we perform FDTD calculations of the field distribution in the proximity to the structures composed of the gold film with nanocylinders on its top (Figs. 5 and 6). The extinction spectra calculated by FDTD (supplementary information, Figures S11–3) are in a very good agreement with the experimental spectra as they reproduce the same spectrum plasmon bands at close spectral positions and with similar evolution due to the changes of the film thickness d_m . The electric field distributions obtained at the resonance position can be seen in the Fig. 5 (resonances A and B) and Fig. 6 (resonance A). Let us focus on nanocylinder with a diameter of 200 nm (Fig. 5). First, except for the 520 nm mode for gold film thickness of $d_m = 30$ and 40 nm, the field profile shows its concentration at the interface between glass and gold film that confirms our assignment to propagating plasmon modes that travel in the limit of large thickness d_m at the glass/gold surface. The electric field amplitude enhancement decreases with the thickness in all the cases (the field is even no more observable for the 520 nm mode). In the second place, remarkably, we observe some field enhancement (with a factor between 5 and 8) at the corner and at the edges of the nanocylinders for all the excited modes and for varied gold film thickness. This can be assigned to the LSP character and to the possible diffraction scattering of counter-propagating PSP modes. This means that in all the cases, a strong field enhancement occurs at the surface of the nanostructures even if the mode is excited at the opposite interface. This is of first importance as such substrate could be efficiently used for enhanced spectroscopy applications as SERS. These behaviours are observed for all

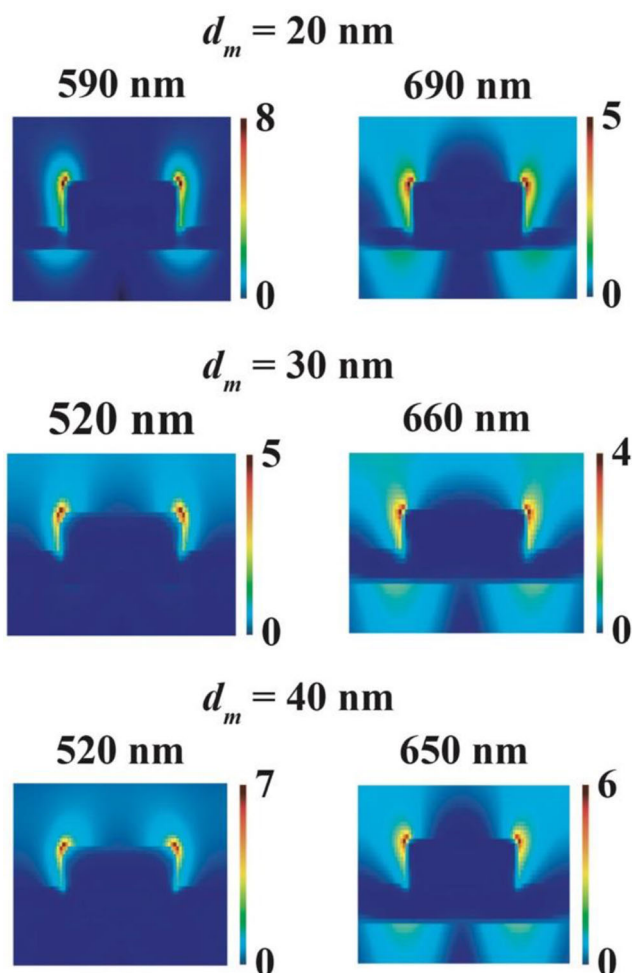


Fig. 5 Electric field distribution around the plasmonic substrate (nanocylinder with a diameter of 200 nm) for three thicknesses, d_m (20, 30, and 40 nm) calculated by FDTD simulations for the resonances A (right column) and B (left column). The spectral position of the plasmon resonance is indicated on the top of each image. On the right of each image, the electric field amplitude enhancement is indicated (the incident field is equal to 1)

diameters as shown on Fig. 6. We can also observe that the field enhancements at the glass/gold interface or at the nanocylinder surface increase with the diameter D , which can be ascribed to the increasing diffraction coupling strength to then fundamental surface plasmon mode TM_0 . A field overlap also occurs for the largest diameter (250 nm) indicating a coupling between adjacent nanocylinders.

We then perform some angular-dependent transmission measurements by tilting the sample in order to control the excitation wave vector and as a consequence to modify the phase matching condition (equation 2). The evolution of the surface plasmon bands with the angle of incidence θ can then be deduced from the acquired spectra. As shown in the Fig. 7, the spectral position of surface plasmon bands is strongly shifted and several band splitting occur. One can also notice the appearance of new bands. In fact, as the incident wave

vector is no more perpendicular to the interface, the angular component of the wave vector, $n_a \cdot \sin[\theta] \cdot \sin[\phi]$, in the equation 2 is no more zero. This induces the splitting of the 2 diffraction orders $(0, \pm 1)$ or $(\pm 1, 0)$ and $(\pm 1, \pm 1)$ in five new diffraction orders: $(0, +1)$ or $(+1, 0)$, $(0, -1)$ or $(-1, 0)$, $(+1, +1)$, $(-1, -1)$ and $(+1, -1)$ or $(-1, +1)$. Such orders intersect the dispersion relation of the TM_0 and TM_1 mode at shifted wavelengths compared to the normal incident angle and for large angles θ , some phase matching can also occur with both these modes (Figure SI4). For instance, the $(0, +1)$ or $(+1, 0)$ and the $(-1, -1)$ modes are blue-shifted whereas the $(0, -1)$ or $(-1, 0)$, $(+1, +1)$ and $(+1, -1)$ or $(-1, +1)$ mode are red-shifted (Figure SI5).

The theoretical positions of these modes are reproduced in the Fig. 7 c and d and are compared to the experimental positions. One can observe a good agreement for the $d_m = 30$ nm thickness (same curve slopes with the angle and similar mode positions). Larger deviations are observed for the $d_m = 20$ nm thickness that can be due to some stronger effects of the nanocylinders on the PSP of the film that cannot be treated as a perturbation anymore. In addition, possible deviation between the simulated film thickness d_m and the experimentally prepared one that has a large effect on the spectral position of PSP resonance. Using such model, nearly all the modes can be assigned to one diffraction coupling via a specific diffraction order. However, some bands (black and grey stars in the Fig. 7 c and d) do not correspond to any diffraction orders. We assume that they can be assigned to hybrid modes formed by the coupling between LSP and PSP as it has been demonstrated previously [1].

With such plasmonic substrate, we are able to tune the plasmon resonance across a wide range of wavelengths in the visible and near infrared part of spectrum from 500 nm up to 900 nm only by tilting the substrate. Such behaviour is not achievable with an array of nanocylinders on dielectric substrate that support non-dispersive pure LSP modes. Moreover, if we irradiate the surface with the investigated structure by the use of a large numerical aperture lens (i.e. 0.9 for a $\times 100$ microscope objective), a wide range of incident angles are included inside the illumination cone (from 0° to nearly 65° for a numerical aperture of 0.9 and a beam propagating in air). Thus, a phase matching should always occur between a fraction of incident optical beam and one of the PSP modes. As a consequence, the excitation of one of the PSP modes should always occur inducing a large field enhancement at the substrate surface. Such property is very important for enhanced optical spectroscopies and it suggests that one single substrate could be optimised in order to provide an enhancement of the spectroscopic signal at multiple excitation wavelengths and thus provide a wavelength independent enhancement.

Fig. 6 Electric field distribution around the plasmonic substrate for four nanocylinder diameters (100, 150, 200 and 250 nm) and three thicknesses, d_m (20, 30 and 40 nm) calculated by FDTD simulations for the resonance A (the spectral position of the plasmon resonance is indicated on the top of each distribution). On the right of each image, the electric field amplitude enhancement is indicated (the incident field is equal to 1)

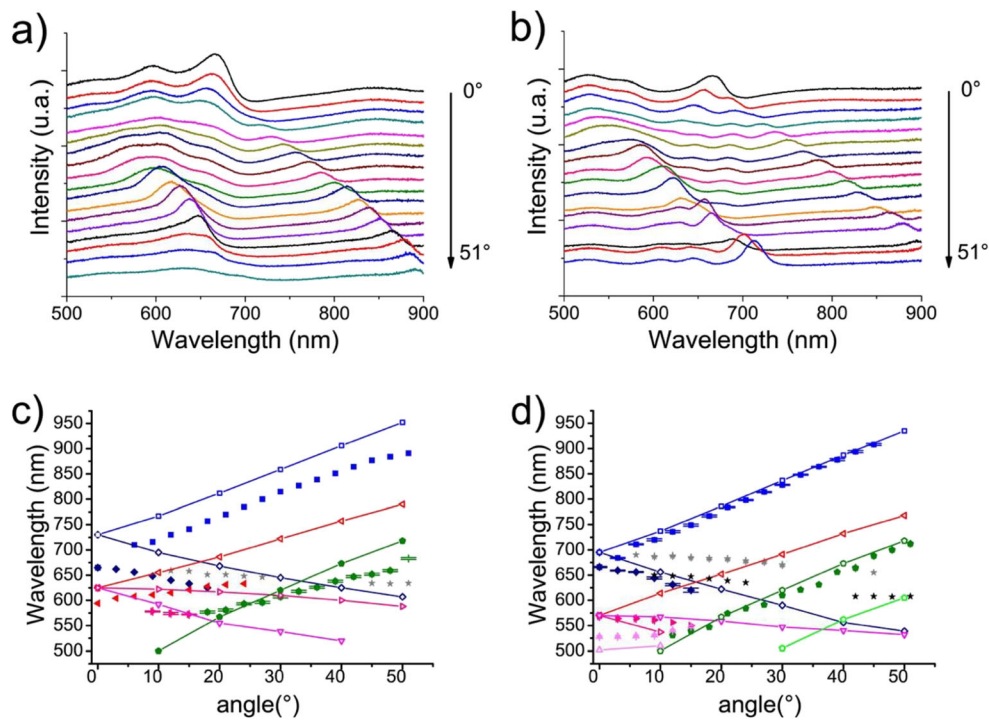
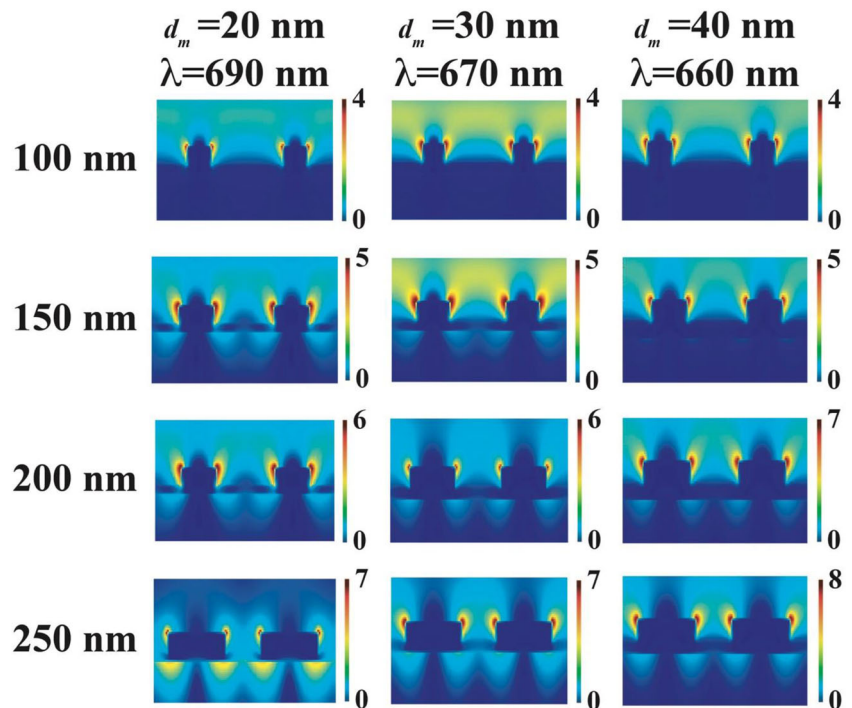


Fig. 7 Evolution of the extinction spectra with the tilting angle from 0° to 51° (step of 3°) for a nanocylinder diameter of 250 nm and a gold film thickness of 20 nm (a) and 30 nm (b). Evolution of the experimental (plain symbols) position of the plasmon bands with the tilting angle (blue squares: $(-1,0)$ or $(0,-1)/TM_0$ mode, dark blue diamonds: $(1,0)$ or $(0,1)/TM_0$ mode, red triangles: $(-1,-1)/TM_0$ mode, pink triangles: $(-1,1)/TM_0$ mode on figure c) and $(1,1)/TM_0$ mode on figure d), green

pentagons: $(-1,0)$ or $(0,-1)/TM_1$ mode, the grey and black stars are unknown modes). The void symbols (connected by plain lines) correspond to the theoretical position calculated with the analytical model (blue squares: $(-1,0)$ or $(0,-1)/TM_0$ mode, dark blue diamonds: $(1,0)$ or $(0,1)/TM_0$ mode, red triangles: $(-1,-1)/TM_0$ mode, dark pink and pink triangles: $(-1,1)/TM_0$ mode and $(1,1)/TM_0$ mode, respectively, green pentagons: $(-1,0)$ or $(0,-1)/TM_1$ mode)

Conclusion

In this paper, we study systematically the optical properties of plasmonic substrates composed of gold nanocylinder grating deposited on a gold thin film depending on the film thickness. We are able to observe and assign several plasmon modes due to the coupling of the diffraction orders defined by the grating with the PSP inside the film. Using the adequate incidence conditions (incident angle, excitation wavelength), several plasmons can be excited simultaneously and tuned on a wide wavelength range taking advantage of the propagative plasmon properties. Moreover, such modes produce large field enhancement at the glass/gold interface but most importantly at the surface of the nanostructures, contrary to PSP modes. This enhancement is similar to the one accessible with localised surface plasmon with nanostructures on dielectric substrates. Thus, these plasmonic substrates combine both advantages of the propagative and localised surface plasmons and could have large applications in enhanced optical spectroscopies. By exploiting their specific plasmonic properties and by optimising their geometrical parameters (grating period, film thickness), we could design a single plasmonic substrate providing plasmon resonances on the whole visible range and as a consequence a nearly constant enhancement for a wide range of excitation wavelengths. Thus, we assume that nanostructure grating on gold film could be used as a multispectral SERS substrate providing a large SERS efficiency on a wide spectral range and that could be used at several wavelengths without losing its enhancement efficiency. Finally, the use of nanoparticle grating can be used to probe the PSP in the gold film. From the mode assignments, we could be able to reconstruct the dispersion relation of the plasmon modes supported by the gold thin film and determine the precise influence of the nanostructures on the propagative plasmon of the film.

Experimental Section

Gold Nanostructures

To produce our plasmonic substrate, a gold thin film is initially deposited on a glass substrate (commercial 0.7-mm-thick glass slide from Lumtec technology, Taiwan) by evaporation process (Plassys, France) with a specific thickness (20, 30, 40 or 50 nm \pm 3 nm). In a second step, the gold nanocylinder arrays were fabricated using electron beam lithography using a Scanning Electron Microscope (Pioneer, Raith). Before e-beam exposure, a 140-nm-thick poly(methyl methacrylate) (PMMA) layer was deposited by spin coating and then patterned using the same e-beam parameters for all substrates and thicknesses. A standard 1:3 ratio of methyl isobutyl ketone (MIBK) and isopropanol (IPA) solution for 60 s is used as a resist development. Finally, 50 \pm 3 nm of gold was deposited by thermal evaporation to produce the nanocylinders. By the

use of a lift-off process upon the immersion in acetone followed by rinsing the PMMA layer is removed resulting in the final structure with gold nanocylinders.

Several arrays were designed with varying the nanocylinder diameters (D) from 80 to 250 nm. The nanocylinder height is fixed at 50 nm. For all diameters D , a constant array periodicity (distance between the centres of the nanocylinders) of 400 nm is maintained in both in plane orthogonal directions to form a square grating. Each array forms a square of 80 \times 80 μm^2 . Scanning electron microscopy (Pioneer, Raith) was performed to ensure the quality of our plasmonic arrays (Fig. 1).

Extinction Spectroscopy

Extinction spectra were recorded with an XploRA confocal Raman microspectrometer (Horiba Scientific) after removing the edge filters. We illuminated the sample in transmission configuration using a non-polarised white lamp. The transmitted light was collected with a low magnification objective (10 \times , numerical aperture of 0.25) in order to preferably collect only the transmitted zero order light beam and no scattered and diffracted light beams. A reference spectrum was also recorded on the area of the sample with the gold thin film without the gold nanocylinders. The extinction spectrum is calculated as the ratio between the transmitted and the reference spectra.

FDTD Simulations

A three-dimensional FDTD method that was implemented in a commercial software from Lumerical Inc. (Canada) was used to calculate the extinction spectra and electric field distributions in the vicinity of the gold nanocylinders on gold film. The geometry of nanocylinder arrays was described by using Cartesian coordinates with the x - and y -axis in the plane and with z -axis perpendicular to the plane of the arrays. The mesh size was 2 nm \times 2 nm \times 2 nm in all the simulations. Convergence checks lead to the conclusion that this mesh size was sufficient for accurate results. Perfectly matched layers (PML) were used as absorbing boundary condition for z -axis to prevent counterfeit reflections [36] and periodic Bloch boundary conditions were applied in the x - and y -direction. The background refractive index was set to 1.00 for air and 1.50 for the glass substrate. Electromagnetic field in the proximity of the nanocylinders was calculated assuming plane wave illumination and normal incidence geometry, with wavelengths varying between 500 and 900 nm. Optical constants of gold were taken from literature [37].

Acknowledgments This work has been partly performed at the “Centrale de Proximité en Nanotechnologies de Paris Nord” (CPN2, 99 Avenue

Jean-Baptiste Clément 93430 Villetaneuse, France) of the Université Paris 13.

Funding Information This work is supported by the grant PIRANEX project (ANR-12-NANO-0016), the Louise project (ANR-15-CE04-0001), and the Nanobiosensor project (ANR-15-CE29-0026) from the French National Research Agency (ANR).

References

- Sarkar M, Besbes M, Moreau J, Bryche JF, Olivéro A, Barbillon G, Coutrot AL, Bartenlian B, Canva M (2015) Hybrid plasmonic mode by resonant coupling of localized plasmons to propagating plasmons in a Kretschmann configuration. *ACS Photonics* 2:237–245
- Mock JJ, Hill RT, Degiron A, Zauscher S, Chilkoti A, Smith DR (2008) Distance-dependent plasmon resonant coupling between a gold nanoparticle and gold film. *Nano Lett* 8:2245–2252
- Mock JJ, Hill RT, Tsai YJ, Chilkoti A, Smith DR (2012) Probing dynamically tunable localized surface plasmon resonances of film-coupled nanoparticles by evanescent wave excitation. *Nano Lett* 12:1757–1764
- Lassiter JB, McGuire F, Mock JJ, Ciraci C, Hill RT, Wiley BJ, Chilkoti A, Smith DR (2013) Plasmonic waveguide modes of film-coupled metallic nanocubes. *Nano Lett* 13:5866–5872
- Wang W, Bai X, Pang Z, Yang H, Qi Y (2019) Investigation of surface plasmons in Kretschmann structure loaded with a silver nano-cube. *Results in Physics* 12:1866–1870
- Wang W, Bai X, Pang Z, Zhu J, Wu Y, Yang H, Qi Y, Wen X (2019) Surface-enhanced Raman scattering by composite structure of gold nanocube-PMMA-gold film. *Opt Mater Express* 9:1872–1881
- Wang W, Zhu J, Wen X, Wu X, Su Y, Tong H, Qi Y, Yang H (2019) Wide range refractive index sensor based on a coupled structure of Au nanocubes and Au film. *Opt Mater Express* 9:3079–3088
- Wang W, Zhu J, Tong H, Yang X, Wu X, Pang Z, Yang H, Qi Y (2019) A theoretical study of a plasmonic sensor comprising a gold nano-disk array on gold film with a SiO₂ spacer. *Chin Phys B* 28:044201
- Chen J, Hu J (2014) Strong coupling between localized and propagating surface plasmon modes in a noncentrosymmetric metallic photonic slab. *J Opt Soc Am B* 31:1600–1606
- Chu Y, Crozier KB (2009) Experimental study of the interaction between localized and propagating surface plasmons. *Opt Lett* 34:244–246
- Sarkar M, Bryche JF, Moreau J, Besbes M, Barbillon G, Bartenlian B, Canva M (2015) *Opt Express* 23:27376–27390
- Felid N, Lau Truong S, Aubard J, Lévi G, Krenn JR, Hohenau A, Leitner A, Aussenegg FR (2004) Gold particle interaction in regular arrays probed by surface enhanced Raman scattering. *J Chem Phys* 120:7141–7146
- Baltar H, Drozdowicz-Tomsia K, Goldys EM (2018) Plasmonic properties of periodic arrays of Ag nanocylinders and dimers, and the effects of an underlying Ag layer. *J Phys Chem C* 122:22083–22093
- Gillibert R, Tafar T, de la Chapelle ML (2017) *Physica Status Solidi A* 214:1600793
- Hohenau A, Krenn JR, Garcia-Vidal FJ, Rodrigo SG, Martin-Moreno L, Beermann J, Bozhevolnyi SI (2007) Spectroscopy and nonlinear microscopy of gold nanoparticle arrays on gold films. *Phys Rev B* 75:085104
- Hohenau A, Krenn JR, Garcia-Vidal FJ, Rodrigo SG, Martin-Moreno L, Beermann J, Bozhevolnyi SI (2007) Comparison of finite-difference time-domain simulations and experiments on the optical properties of gold nanoparticle arrays on gold film. *J Opt A Pure Appl Opt* 9:S366–S371
- Banville FA, Moreau J, Sarkar M, Besbes M, Canva M, Charette PG (2018) Spatial resolution versus contrast trade-off enhancement in high-resolution surface plasmon resonance imaging (SPRI) by metal surface nanostructure design. *Opt Express* 26:10616–10630
- Toma M, Knoll W, Dostalek J (2012) *Plasmonics* 7:293–299
- Indutnyi IZ, Ushenin YV, Min'ko VI, Shepeliavyi PE, Lukaniuk AA, Korchovyi AA, Khrystosenko RV (2017) Nanostructured Au chips with enhanced sensitivity for sensors based on surface plasmon resonance. *Ukr J Phys* 62:365–371
- Toma M, Toma K, Adam P, Homola J, Knoll W, Dostalek J (2012) *Opt Express* 20:14042–14053
- Bryche JF, Gillibert R, Barbillon G, Gogol P, Moreau J, de la Chapelle ML, Bartenlian B, Canva M (2016) *Plasmonics* 11:601–608
- Bryche JF, Gillibert R, Barbillon G, Sarkar M, Coutrot AL, Hamouda F, Aassime A, Moreau J, de la Chapelle ML, Bartenlian B, Canva M (2015) *J Mater Sci* 50:6601–6607
- Bryche JF, Tsigara A, Béliet B, de la Chapelle ML, Canva M, Bartenlian B, Barbillon G (2016) *Sensors Actuators B* 228:31–35
- Magno G, Béliet B, Barbillon G (2017) Gold thickness impact on the enhancement of SERS detection in low-cost Au/Si nanosensors. *J Mater Sci* 52:13650–13656
- Gillibert R, Sarkar M, Bryche JF, Yasukuni R, Moreau J, Besbes M, Barbillon G, Bartenlian B, Canva M, de la Chapelle ML (2016) *Nanotechnology* 27:115202
- Gillibert R, Sarkar M, Moreau J, Besbes M, Canva M, Lamy de la Chapelle M, Phys J (2016) *Chem C* 120:27562–27570
- Haynes CL, Van Duyne RP (2003) Plasmon-sampled surface-enhanced Raman excitation spectroscopy†. *J Phys Chem B* 107:7426–7433
- Le Ru EC, Grand J, Felidj N, Aubard J, Levi G, Hohenau A, Krenn JR, Blackie E, Etchegoin PG (2008) *J Phys Chem C* 112:8117–8121
- Mc Farland AD, Young MA, Dieringer JA, Van Duyne RP (2005) Wavelength-scanned surface-enhanced Raman excitation spectroscopy. *J Phys Chem B* 109:11279–11285
- Felidj N, Aubard J, Levi G, Krenn JR, Hohenau A, Schider G, Leitner A, Aussenegg FR (2003) Optimized surface-enhanced Raman scattering on gold nanoparticle arrays. *Appl Phys Lett* 82:3095–3097
- Felidj N, Aubard J, Levi G, Krenn JR, Salerno M, Schider G, Lamprecht B, Leitner A, Aussenegg FR (2002) Controlling the optical response of regular arrays of gold particles for surface-enhanced Raman scattering. *Phys Rev B* 65:075419
- Guillot N, de la Chapelle ML (2012) *J Quant Spectrosc Radiat Transf* 113:2321–2333
- Guillot N, Lamy de la Chapelle M (2012) *J Nanophotonics* 6:64506
- Gillibert N, Huang JQ, Zhang Y, Fu WL, de la Chapelle ML (2018) *Trends Anal Chem* 105:185–190
- Gillibert N, Huang JQ, Zhang Y, Fu WL, de la Chapelle ML (2018) *Trends Anal Chem* 105:166–172
- Oskooi A, Johnson S (2011) Distinguishing correct from incorrect PML proposals and a corrected unsplit PML for anisotropic, dispersive media. *J Comp Phys* 230:2369–2377
- Johnson PB, Christy RW (1972) Optical constants of the noble metals. *Phys Rev B* 6:4370–4379

Publisher's Note Springer Nature remains neutral with regard to jurisdictional claims in published maps and institutional affiliations.